Electrical nucleation and detection of single 360° homochiral Néel domain walls measured using the anomalous Nernst effect

Murat Cubukcu, Deepak Venkateshvaran, Angela Wittmann, Shu-Jen Wang, Riccardo Di Pietro, Stephane Auffret, Laurent Vila, Joerg Wunderlich, and Henning Sirringhaus

Citation: Appl. Phys. Lett. **112**, 262409 (2018); doi: 10.1063/1.5040321
View online: https://doi.org/10.1063/1.5040321
View Table of Contents: http://aip.scitation.org/toc/apl/112/26
Published by the American Institute of Physics

Electrical nucleation and detection of single 360° homochiral Néel domain walls measured using the anomalous Nernst effect

Murat Cubukcu,[1,a)] Deepak Venkateshvaran,[1] Angela Wittmann,[1] Shu-Jen Wang,[1] Riccardo Di Pietro,[2] Stephane Auffret,[3] Laurent Vila,[3] Joerg Wunderlich,[2] and Henning Sirringhaus[1]

[1]*Cavendish Laboratory, University of Cambridge, J. J. Thomson Avenue, Cambridge CB3 0HE, United Kingdom*
[2]*Hitachi Cavendish Laboratory, J. J. Thomson Avenue, Cambridge CB3 0HE, United Kingdom*
[3]*SPINTEC, CEA, CNRS and Université Grenoble Alpes, 17 rue des Martyrs, 38054 Grenoble, France*

(Received 16 May 2018; accepted 19 June 2018; published online 28 June 2018)

Using a thermoelectric measurement, we demonstrate the nucleation and detection of a single 360° homochiral Néel domain wall (DW), formed by an independently nucleated pair of 180° Néel DWs having the same helicity in a perpendicular magnetic anisotropy track. The DW formation is governed by strong interfacial Dzyaloshinskii-Moriya interaction (DMI) and detected at room temperature using the anomalous Nernst effect (ANE). A large DMI can be generated at an interface where the symmetry is broken between a material having a large spin-orbit coupling and a thin ferromagnetic layer. The ANE voltage, $V_{ANE} \propto \nabla T \times M$, is sensitive to the magnitude of the out-of-plane magnetization M through a confined in-plane temperature gradient ∇T and allows for the direct thermoelectrical detection of the DW position with nanoscale accuracy along the track. Here, we present evidence that independently nucleated pairs of 180° Néel DWs in microwire devices can be brought together by an applied magnetic field to form a 360° homochiral Néel DW. Subsequently, we show that a strong magnetic field needs to be applied in order to annihilate the 360° DW due to the strong interfacial DMI in our Pt/Co(0.6nm)/AlO_x multilayers. In addition to enabling a high magnetic storage and data transfer rate with low power consumption in novel computational and storage devices, such DWs facilitate a reduction in bit size down to a few nanometers with metastability. *Published by AIP Publishing.* https://doi.org/10.1063/1.5040321

The constant rise in data volume and complexity in today's society is currently raising huge challenges to store and process information. Dense and low power consumption mass storage devices, as well as stand-alone and embedded memories such as non-volatile random access memories (RAMs), are required. Fast non-volatile RAM that can be written with a very low energy is a credible candidate to replace static RAM (SRAM) in cache memories and integrate non-volatility in the core of future processors. This would considerably reduce power consumption as well as pave the way towards normally-off-instantly-on computers. Some very innovative solutions for two types of applications in random access memories, such as non-volatile magnetic RAM (MRAM) memory[1–3] as well as mass storage, were recently proposed.[4] Recent advances led to several proposals for storage class magnetic memories that could form a solid state replacement for hard disks at equivalent manufacturing cost in the data storage industry. One of the most famous proposals is the domain wall (DW) racetrack memory. Racetrack memory involves moving magnetic DWs—the boundaries between regions of opposite magnetization—along a nanowire using spin-polarized current pulses and reading the magnetization at well-defined positions along the wire.[4] This system also offers the opportunity to make logical operations by manipulating DWs.

DWs are a particular example of a magnetization pattern which can be used to store information using magnetism in what would otherwise be the uniform magnetization of a conventional ferromagnetic material. However, despite large research efforts on DWs in recent years, real proof-of-concept of functional devices are still missing. Several fundamental issues have impeded the practical realization of such devices, namely, the large current density needed to move the DWs that leads to large writing energies, heating and reliability issues, and the large DW pinning that leads to stochasticity in the DW position at rest. Some of these aforementioned issues are even known to induce errors in the writing process. Besides directly demonstrating the interaction of charge and spin current within the magnetization texture present in nanowire DW devices, their careful electrical characterization holds useful information for its future implementation in emerging technologies. The existing electrical detection approach using the anomalous Hall effect (AHE) is limited to specific device architectures such as Hall crosses,[5,6] and the work presented here adds another seldomly used yet functional device-based approach based on the anomalous Nernst effect (ANE).

We have recently demonstrated precise track position and motion detection of a single propagating DW in a perpendicular magnetic anisotropy (PMA) material with nanoscale resolution, using the thermoelectrical analogue of the AHE, the ANE.[7] The ANE voltage, $\boldsymbol{V}_{ANE} \propto \nabla \boldsymbol{T} \times \boldsymbol{M}$, is an integral over the local electromotive force along the track and is sensitive to the out-of-plane magnetization M through a confined thermal gradient ∇T. For a constant ∇T over the wire length, V_{ANE} depends linearly on DW position,

a)mc2026@cam.ac.uk

thus allowing direct thermoelectrical detection of the DW position with nanoscale accuracy.

In this work, we report electrically the nucleation and detection of a single 360° homochiral Néel DW through ANE in a PMA track with a strong interfacial Dzyaloshinskii-Moriya interaction (DMI). The DMI is known to be a direct manifestation of spin-orbit coupling (SOC) in systems with broken inversion symmetry.[8,9] A large DMI can be generated at the interface with a broken symmetry between a material having a large SOC (e.g., Pt or Ta) and a thin ferromagnetic layer.[10–14] It has been shown that the DMI can change the structure of DWs from conventional Bloch configurations into chiral Néel geometries,[15] controlling the direction of propagation and increasing the velocity of the DW in racetrack structures dramatically.[16] DMI also leads to the creation of nanometer-scale topologically stable magnetic skyrmions that can be manipulated by extremely low current densities.[13,17–25]

We present evidence that, when brought together by an applied magnetic field, two independently nucleated 180° Néel DWs with the same helicity create a 360° homochiral Néel DW. When the two 180° Néel DWs meet, they are difficult to annihilate in our Pt/Co(0.6 nm)/AlO_x multilayers due to the presence of a strong interfacial DMI, and require large applied magnetic fields (>0.35 T) directed along the domain magnetization. The presence of a single 360° Néel DW is detected by assuming that the 360° Néel DW is a nucleation center generated when applying a magnetic field opposite to the magnetization orientation of our magnetized wire. In this case, two oppositely propagating 180° Néel DWs are responsible for the magnetization reversal of the whole wire, and the nucleation field is found to be significantly reduced compared to a fully saturated wire. This is because the nucleation process before and after the creation of the 360° Néel DW is qualitatively different.

The Néel wall gives rise to up and down magnetic moments along the whole length of the 180° Néel DW, separated by the DW width Δ. DW width is on the order of $\Delta \cong \pi\sqrt{AK_{\text{eff}}^{-1}}$, where A is the exchange stiffness and K_{eff} is the effective anisotropy constant including the perpendicular demagnetizing field in the local approximation. Δ is typically several nanometres in such systems.[15] A single 360° homochiral Néel DW can be formed from pairs of 180° Néel DWs with the same helicity but demonstrates qualitatively distinct behavior from their constituent 180° Néel DWs [see Fig. 1(a)]. To enable electrical nucleation and detection of such DWs, ANE measurements were carried out.

Figure 1(b) shows a scanning electron microscope (SEM) image of a fabricated device, consisting of a Pt/Co/AlO_x wire with a notch in the center sandwiched between two adjacent Pt heater lines. It contains Au nucleation strip lines crossing the left and right contact area of the magnetic wire. Ta(3 nm)/Pt(3 nm)/Co(0.6 nm)/AlO_x(2 nm) magnetic microwires were defined using electron beam lithography and comprise a 1 μm wide and either a 60 μm or 120 μm long wire. The multilayers were deposited on a thermally oxidized silicon wafer by DC magnetron sputtering. After deposition, the samples were oxidized at a pressure of 3×10^{-3} mbar and a radio-frequency power of 10 W in order to induce strong perpendicular anisotropy. The process was identical

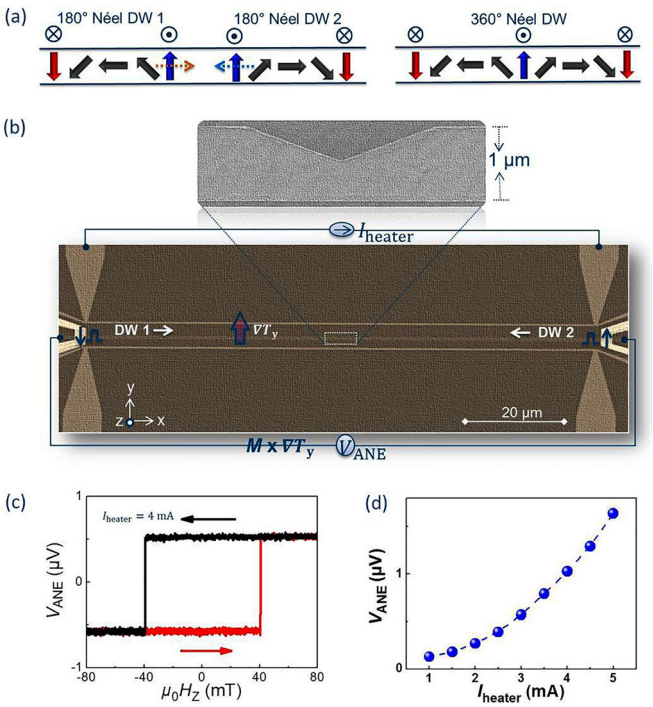

FIG. 1. Single 360° homochiral Néel DW, devices and ANE reversal loops. (a) Illustration of a 360° homochiral Néel DW created from 2 × 180° Néel DWs. (b) SEM image of the device with microwire, two Pt heater lines, Au nucleation strip lines, and a schematic representation of the electrical measurement setup. V_{ANE} and I_{heater} represent the ANE voltage and heater current, respectively. (c) V_{ANE} as a function of applied perpendicular magnetic field (H_z) to the device. The arrows show the sweep direction of H_z. (d) V_{ANE} as a function of I_{heater}. The dashed line shows a quadratic fit.

to that published earlier.[26] The electrical contacts/heater lines-Pt(25 nm) and the nucleation stripe lines-Cr(10 nm)/Au(100 nm) were defined in a lift-off process using electron beam lithography and sputter deposition and evaporation, respectively. Two 500 nm wide Pt heater wires were patterned 3 μm above and 3 μm below the central magnetic microwire. The magnetic parameters in such systems for Pt/Co/AlO_x multilayers are the exchange stiffness $A \cong 16$ pJ/m, saturation magnetization $M_s \cong 1.1$ MA/m, perpendicular anisotropy $K \cong 1.3$ MJ/m^3, and DMI parameter $D \cong 2.6$ mJ/m^2.[27,28] In-plane thermal gradients perpendicular to the long-axis of the microwires are generated by electrical heater current lines running parallel to the microwires. An oscillating heat gradient was generated by the application of AC heater currents of 1 mA up to 10 mA with the frequency $f_{heat} = 79$ Hz. V_{ANE} was measured using lock-in detection at the second harmonic at room temperature. DW injection was carried out by applying a current pulse to these strip lines. The application of 5-ms-long nucleation pulse of 90 mA to the strip line generates an Oersted field which forms a reversed magnetized domain with a single DW present on the left-hand side (DW 1) and right-hand side (DW 2) of the magnetic wire, respectively.

Figure 1(c) shows the typical ANE voltage while sweeping the external magnetic field in the direction perpendicular to the substrate and the microwire $\mu_0 H_z$ and applying a heater current $I_{heater} = 4$ mA (heater power $P_{heater} = 62.4$ mW) to the heater line at room temperature. The magnetization reversal is reflected in a hysteretic behaviour in V_{ANE}

with the square loop (coercive field $\mu_0 H_{\text{coercive}} \cong 40.5\,\text{mT}$) indicating magnetization reversal is governed by fast DW motion. V_{ANE} scales quadratically with increasing I_{heater} [see Fig. 1(d)] and hence linearly with the applied P_{heater} and ∇T, as expected for a thermoelectric signal.[7]

Figure 2(a) shows the illustration of the state of the magnetization using SEM images in our microwire device step-by-step from a saturated state to the state of a single 360° Néel DW created from independently nucleated pairs of 180° Néel DWs with the same helicity. Figure 2(b) shows the variation of the ANE signal when the DW 1 creeps along the magnetic microwire driven by a magnetic field. Before the nucleation of DW 1, a perpendicular positive saturation field of 1 T was applied to saturate the microwire magnetization. The field was then swept from zero to −50 mT. The DW 1 is nucleated at $\mu_0 H_{\text{nuc}} \cong -17\,\text{mT}$ and at this field V_{ANE} sharply rises from $V_{\text{ANE}} \cong 0.5\,\mu\text{V}$ to a nearly zero value. Here, a reversed domain has first nucleated at the microwire and then propagated to the notch centered between the two contacts where it remained pinned. The peak at the beginning of the plateau is induced by electrical crosstalk from the nucleation pulse (N.P). DW 1 then depins from the notch around −23 mT and continues propagation through the remaining part of the microwire, completing the magnetization reversal ($V_{\text{ANE}} \cong -0.5\,\mu\text{V}$). Figure 2(c) shows a minor loop allowing pinned DW 1 at the notch. Note that the similar behavior has also been observed on the right-hand side for DW 2 of the magnetic wire. Once DW 1 is nucleated, propagated, and pinned at the notch ($V_{\text{ANE}} \cong 0\,\mu\text{V}$), DW 2 can then be nucleated and propagated with increasing magnetic field from zero until the notch where the two 180° Néel DWs meet. Here, they merge into a 360° Néel DWs ($V_{\text{ANE}} \cong -0.5\,\mu\text{V}$) [Fig. 2(d), black curve].

In order to quantify a single 360° Néel DW created in the microwire, we compare the coercive field in the presence of the 360° Néel DW to the coercive field of a homogeneously saturated sample. We sweep the magnetic field in the direction opposite to the magnetization orientation from −50 mT to 50 mT. A single 360° Néel DW can then be separated into two 180° at $\mu_0 H_{\text{nuc}\,(360°)} \cong 36.5\,\text{mT}$. The microwire now switches clearly at a field lower than the coercive field of the major loop [Fig. 2(a)], i.e., $\mu_0 H_{\text{nuc}\,(360°)} < \mu_0 H_{\text{coercive}}$ which show the magnetization reversal process is now governed by the propagation of two separated 180° Néel DWs [Fig. 2(d), blue curve]. Figure 3(a) shows the nucleation field $\mu_0 H_{\text{nuc}}$ as a function of $\mu_0 H_z$ for $\mu_0 H_z \leq -60\,\text{mT}$ after nucleating two 180° Néel DWs every time. For $\mu_0 H_z \geq -35\,\text{mT}$, the nucleation field is stable around 36.5 mT which indicates the stabilization of a 360° Néel DW. For smaller negative applied $\mu_0 H_z$, the two 180° Néel DWs do not yet meet at the notch [Fig. 2(a) state (4)] or $\mu_0 H_z$ is not yet enough to stabilize 360° Néel DW.

In order to measure the annihilation field, a single 360° Néel DW was created at $\mu_0 H_z = -60\,\text{mT}$ and then the magnetic field was ramped to a maximum field $-\mu_0 H_{\text{max}}$. $-H_{\text{max}}$ is the large applied magnetic field directed along the domain magnetization in the same direction as the −60 mT generation field. The magnetic field is then swept back to a positive applied magnetic field at 60 mT so that the nucleation field $\mu_0 H_{\text{nuc}}$ can be measured. This is repeated for different $-\mu_0 H_{\text{max}}$ after creating a 360° Néel DW every time. Figure 3(a) shows the dependence of the measured $\mu_0 H_{\text{nuc}}$ on the $-\mu_0 H_{\text{max}}$. When $-\mu_0 H_{\text{max}} > 0.35\,\text{T}$, the magnetic field is large enough to annihilate the 360° Néel DW and the nucleation field sharply rises from ∼36.5 mT to ∼40.5 mT [Fig. 3(d), inset]. The sharp rise is caused by the nucleation process and is qualitatively different from that after full saturation has been achieved.[29] Once a single 360° Néel DW is annihilated, the reversal process is governed by reversed domain nucleation and propagation as on the major loop [Fig. 1(c)] rather than propagation of two 180° DWs. The error bar in the figures reflects the distribution of fields due to thermal activation for all events while repeating the

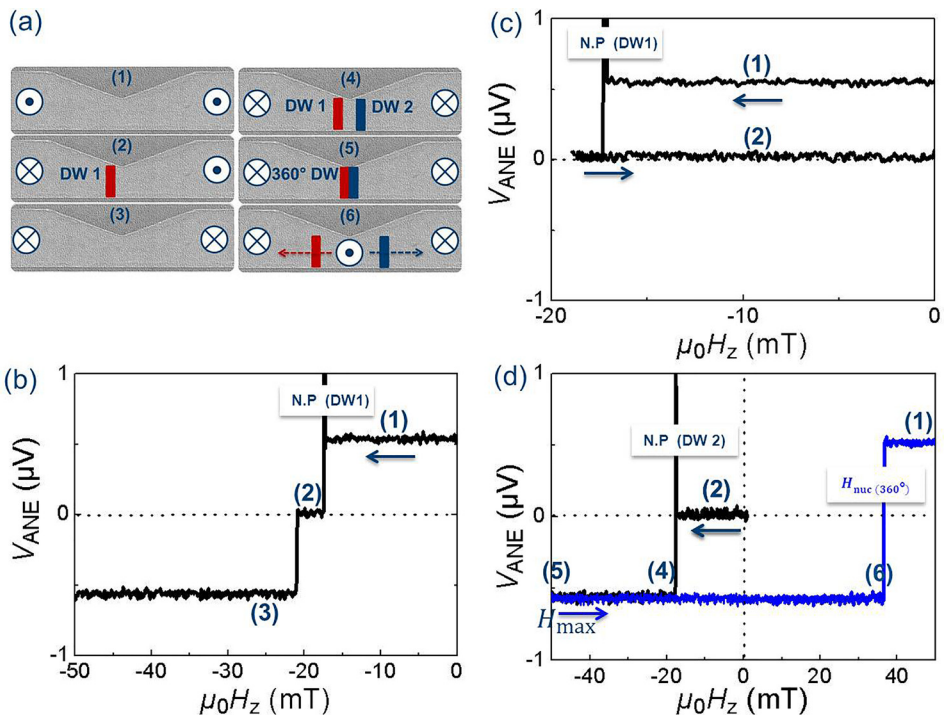

FIG. 2. Nucleation and detection of a single 360° Néel DW. (a) Illustration of the state of the magnetization using SEM images of our microwire device step by step from a saturated state (1) to the state of a single 360° Néel DW created from an independently nucleated pair of 180° Néel DWs (5) and then separating them into two 180° Néel DWs (6). (b) ANE voltage measurement of the 1 μm wide PMA wire before and after DW 1 creation and detection while sweeping a magnetic field. (c) The minor loop shows clearly pinned DW 1 at the notch. (d) The formation of a single 360° Néel DW from an independently nucleated pair of 180° Néel DWs with the same helicity.

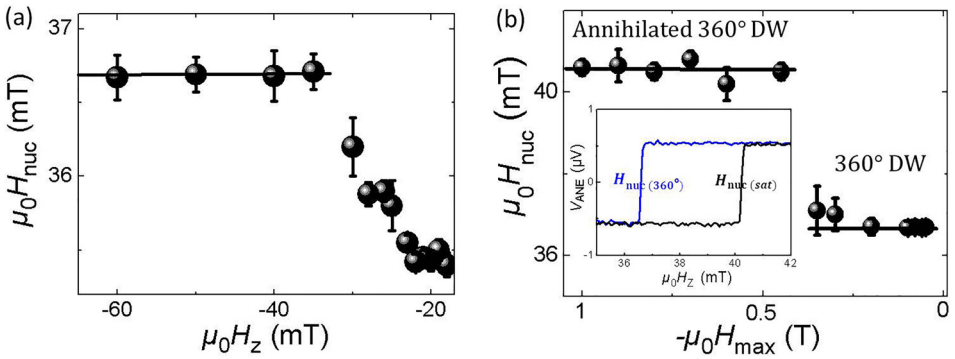

FIG. 3. Annihilation field of a single 360° Néel DW. (a) Nucleation field $\mu_0 H_{nuc}$ as a function of the $\mu_0 H_z$ for $\mu_0 H_z \leq -60$ mT after nucleating two 180° Néel DWs every time. (b) Nucleation field $\mu_0 H_{nuc}$ as a function of a maximum field $-\mu_0 H_{max}$ where two different regimes are measured, i.e., 360° Néel DW and annihilated 360° Néel DW. Inset shows nucleation field of a microwire with 360° Néel DW $\mu_0 H_{nuc\,(360°)}$ (blue curve) and after 360° Néel DW is annihilated $\mu_0 H_{nuc\,(sat)}$ (black curve). A total of 10 nucleation fields were averaged to determine $\mu_0 H_{nuc}$.

experiments. This observed difference of fields is obviously much larger.

The formation of a single 360° homochiral Néel DW takes place when two 180° Néel DWs of the same helicity merge together by a magnetic field in the presence of DMI. It is unable to annihilate, since an energy barrier must be overcome when the wall core rotates out of the easy direction defined by the combination of anisotropy and DMI.[29,30] The stability of two 180° Néel DWs in the 360° Néel DW depends on the magnitude of the DMI, and the annihilation field of the 360° Néel DW is a direct evaluation of this DMI.[31] A strong magnetic field (>0.35 T) has to be applied in order to annihilate the 360° Néel DW because of the strong interfacial DMI in our Pt/Co(0.6 nm)/AlO_x multilayers. The high DMI in these heterostructures was previously confirmed through measurements using a scanning nanomagnetometer based on the Nitrogen-Vacancy defect in diamond ($D \cong 2.6\,\mathrm{mJ/m^2}$) by Tetienne *et al.*[27] and using magneto-optical Kerr microscopy ($D \cong 2.2\,\mathrm{mJ/m^2}$) by Pizzini *et al.*[28]

The formation of 360° DWs in Co and Permalloy with in-plane magnetized thin film wires was demonstrated in the past by successively injecting two 180° DWs into the wire.[32–34] The annihilation and dissociation of 360° DWs was demonstrated by applying a magnetic field parallel to the wire, showing that annihilation fields were several times higher than the dissociation field. For a 150 nm wide Co wire, the magnetic field for annihilation of 360° DWs was around 70 mT. The 360° homochiral Néel DWs shown in our work are much more stable than the a-chiral walls studied so far. The current-driven manipulation and motion of 360° homochiral Néel DWs together with their thermal stability are interesting topics for future exploration towards the ultimate goal of using such domain walls in spintronic racetrack memories.

In conclusion, we demonstrate the electrical nucleation and detection of a nanoscale single 360° homochiral Néel DW in a PMA material using a detection scheme that is the thermoelectrical analogue of the AHE, namely, the ANE. This detection scheme eliminates the need for using Hall crosses and is a powerful complementary technique to characterize domain walls along the track using temperature gradients, without the need for a flowing current. Once created, a single 360° Néel DW is difficult to annihilate with high magnetic field for topological reasons, thus demonstrating its potential for use in skyrmion-based spintronic devices.[13,35] Furthermore, a single skyrmion can be nucleated in magnetic wire devices from a 360° Néel DW by applying an in-plane electric current in a rectangular shaped geometry.[36] Finally, ANE detection can potentially provide a simple and powerful electrical detection to precisely track the position and manipulation of magnetic objects in PMA nanostructures.

Funding from the ERC Synergy Grant SC2 (Grant No. 610115) is acknowledged. We gratefully acknowledge P. E. Roy and R. Lebrun for fruitful discussions.

[1]A. D. Kent and D. C. Worledge, Nat. Nanotechnol. **10**, 187–190 (2015).
[2]M. Cubukcu, O. Boulle, M. Drouard, K. Garello, C. O. Avci, I. M. Miron, J. Langer, B. Ocker, P. Gambardella, and G. Gaudin, Appl. Phys. Lett. **104**, 042406 (2014).
[3]M. Cubukcu, O. Boulle, N. Mikuszeit, C. Hamelin, T. Brächer, N. Lamard, M.-C. Cyrille, L. Buda-Prejbeanu, K. Garello, I. M. Miron, O. Klein, G. De Loubens, V. V. Naletov, J. Langer, B. Ocker, P. Gambardella, and G. Gaudin, IEEE Trans. Magn. **54**, 9300204 (2018).
[4]S. S. P. Parkin, M. Hayashi, and L. Thomas, Science **320**, 190–194 (2008).
[5]J. Wunderlich, D. Ravelosona, C. Chappert, F. Cayssol, V. Mathet, J. Ferré, J.-P. Jamet, and A. Thiaville, IEEE Trans. Magn. **37**, 2104 (2001).
[6]S. F. Zhang, W. L. Gan, J. Kwon, F. L. Luo, G. J. Lim, J. B. Wang, and W. S. Lew, Sci. Rep. **6**, 24804 (2016).
[7]P. Krzysteczko, J. Wells, A. F. Scarioni, Z. Soban, T. Janda, X. Hu, V. Saidl, R. P. Campion, R. Mansell, J. Lee, R. P. Cowburn, P. Nemec, O. Kazakova, J. Wunderlich, and H. W. Schumacher, Phys. Rev. B **95**, 220410(R) (2017).
[8]I. Dzyaloshinsky, J. Phys. Chem. Solids **4**, 241 (1958).
[9]T. Moriya, Phys. Rev. **120**, 91 (1960).
[10]S. Emori, U. Bauer, S.-M. Ahn, E. Martinez, and G. S. D. Beach, Nat. Mater. **12**, 611–616 (2013).
[11]K.-S. Ryu, L. Thomas, S. H. Yang, and S. S. P. Parkin, Nat. Nanotechnol. **8**, 527–533 (2013).
[12]S. Meckler, N. Mikuszeit, A. Preßler, E. Y. Vedmedenko, O. Pietzsch, and R. Wiesendanger, Phys. Rev. Lett. **103**, 157201 (2009).
[13]A. Fert, V. Cros, and J. Sampaio, Nat. Nanotechnol. **8**, 152–156 (2013).
[14]M. Cubukcu, J. Sampaio, K. Bouzehouane, D. Apalkov, A. V. Khvalkovskiy, V. Cros, and N. Reyren, Phys. Rev. B **93**, 020401(R) (2016).
[15]A. Thiaville, S. Rohart, É. Jué, V. Cros, and A. Fert, Europhys. Lett. **100**, 57002 (2012).
[16]S. S. P. Parkin and S. H. Yang, Nat. Nanotechnol. **10**, 195–198 (2015).
[17]J. Sampaio, V. Cros, S. Rohart, A. Thiaville, and A. Fert, Nat. Nanotechnol. **8**, 839–844 (2013).
[18]U. K. Robler, A. N. Bogdanov, and C. Pfleiderer, Nature **442**, 797–801 (2006).
[19]S. Mühlbauer, B. Binz, F. Jonietz, C. Pfleiderer, A. Rosch, A. Neubauer, R. Georgii, and P. Böni, Science **323**, 915–919 (2009).
[20]N. Nagaosa and Y. Tokura, Nat. Nanotechnol. **8**, 899–911 (2013).

[21]C. Moreau-Luchaire, C. Moutafis, N. Reyren, J. Sampaio, C. A. F. Vaz, N. Van Horne, K. Bouzehouane, K. Garcia, C. Deranlot, P. Warnicke, P. Wohlhüter, J.-M. George, M. Weigand, J. Raabe, V. Cros, and A. Fert, Nat. Nanotechnol. **11**, 444–448 (2016).
[22]S. Woo, K. Litzius, B. Krüger, M.-Y. Im, L. Caretta, K. Richter, M. Mann, A. Krone, R. M. Reeve, M. Weigand, P. Agrawal, I. Lemesh, M.-A. Mawass, P. Fischer, M. Kläui, and G. S. D. Beach, Nat. Mater. **15**, 501–506 (2016).
[23]K. Litzius, I. Lemesh, B. Krüger, P. Bassirian, L. Caretta, K. Richter, F. Büttner, K. Sato, O. A. Tretiakov, J. Förster, R. M. Reeve, M. Weigand, I. Bykova, H. Stoll, G. Schütz, G. S. D. Beach, and M. Kläui, Nat. Phys. **13**, 170–175 (2017).
[24]F. Büttner, I. Lemesh, M. Schneider, B. Pfau, C. M. Günther, P. Hessing, J. Geilhufe, L. Caretta, D. Engel, B. Krüger, J. Viefhaus, S. Eisebitt, and G. S. D. Beach, Nat. Nanotechnol. **12**, 1040–1044 (2017).
[25]D. Maccariello, W. Legrand, N. Reyren, K. Garcia, K. Bouzehouane, S. Collin, V. Cros, and A. Fert, Nat. Nanotechnol. **13**, 233–237 (2018).
[26]B. Rodmacq, A. Manchon, C. Ducruet, S. Auffret, and B. Dieny, Phys. Rev. B **79**, 024423 (2009).
[27]J.-P. Tetienne, T. Hingant, L. J. Martinez, S. Rohart, A. Thiaville, L. Herrera Diez, K. Garcia, J.-P. Adam, J.-V. Kim, J.-F. Roch, I. M. Miron, G. Gaudin, L. Vila, B. Ocker, D. Ravelosona, and V. Jacques, Nat. Commun. **6**, 6733 (2015).
[28]S. Pizzini, J. Vogel, S. Rohart, L. D. Buda-Prejbeanu, E. Jué, O. Boulle, I. M. Miron, C. K. Safeer, S. Auffret, G. Gaudin, and A. Thiaville, Phys. Rev. Lett. **113**, 047203 (2014).
[29]M. J. Benitez, A. Hrabec, A. P. Mihai, T. A. Moore, G. Burnell, D. McGrouther, C. H. Marrows, and S. McVitie, Nat. Commun. **6**, 8957 (2015).
[30]A. Hubert and R. Scha fer, *Magnetic Domains—The Analysis of Magnetic Microstructures* (Springer, 1998).
[31]R. Hiramatsu, K.-J. Kim, Y. Nakatani, T. Moriyama, and T. Ono, Jpn. J. Appl. Phys., Part 1 **53**, 108001 (2014).
[32]M. D. Mascaro and C. A. Ross, Phys. Rev. B **82**, 214411 (2010).
[33]Y. Jang, S. R. Bowden, M. Mascaro, J. Unguris, and C. Ross, Appl. Phys. Lett. **100**, 062407 (2012).
[34]J. Zhang, S. A. Siddiqui, P. Ho, J. A. Currivan-Incorvia, L. Tryputen, E. Lage, D. C. Bono, M. A. Baldo, and C. A. Ross, New J. Phys. **18**, 053028 (2016).
[35]X. Zhang, M. Ezawa, and Y. Zhou, Sci. Rep. **5**, 9400 (2015).
[36]J. Iwasaki, M. Mochizuki, and N. Nagaosa, Nat. Nanotechnol. **8**, 742–747 (2013).